Transport of sputtered neutral particles

G. J. Parker,[1] W. N. G. Hitchon,[2] and D. J. Koch[3]
[1]*Lawrence Livermore National Laboratory, P.O. Box 808, L-418, Livermore, California 94550*
[2]*Engineering Research Center for Plasma Aided Manufacturing, University of Wisconsin, Madison, Wisconsin 53706*
[3]*Motorola, Inc., 5005 East McDowell Road, Phoenix, Arizona 85008*
(Received 14 February 1994; revised manuscript received 17 October 1994)

The initial deposition rate of sputtered material along the walls of a trench is calculated numerically. The numerical scheme is a nonstatistical description of long-mean-free-path transport in the gas phase. Gas-phase collisions are included by using a "transition matrix" to describe the particle motion, which in the present work is from the source through a cylindrical chamber and into a rectangular trench. The method is much faster and somewhat more accurate than Monte Carlo methods. Initial deposition rates of sputtered material along the walls of the trench are presented for various physical and geometrical situations and the deposition rates are compared to other computational and experimental results.

PACS number(s): 05.20.Dd

I. INTRODUCTION

In this paper we describe a nonstatistical technique for describing transport of sputtered particles and use it to calculate the initial deposition rate of sputtered material inside a trench. Sputtering metal and other material onto substrates is a technique of great technological importance. The procedure described here in essence extends calculations of initial sputtering deposition rates to include gas phase collisions in a nonstatistical scheme [1].

In the past, calculations of the transport of sputtered particles have been done using Monte Carlo (MC) and direct simulation Monte Carlo (DSMC) methods [2–8], which are statistical in nature. Simulation "particles" are followed using the computer. They are allowed to have collisions, which are introduced "randomly" as determined by a random number generator. When sufficient particles have been followed, the physical behavior of the real system can be estimated by averaging the behavior of the simulation particles.

To obtain accurate predictions it is necessary to follow large numbers of particles. This makes the MC method computationally intensive. The method described here is usually at least two orders of magnitude faster than MC calculations while providing greater accuracy. It is nonstatistical in nature — no random numbers are used. Instead a "transition matrix" is constructed which contains the probability of particles which scatter in one location having their next "scatter" at any other location. These scatters can be with particles in the gas phase or with the chamber walls.

In DSMC simulations [6–8] a self-consistent transfer of momentum from the sputtered material to the background gas can be modeled, which is also the case in the transition matrix approach. However, the DSMC as described in Ref. [8] uses cell sizes that are comparable to the mean free path of the sputtered atoms. In the case presented here, the mean free path is comparable to the system size and so the DSMC algorithm would have to be altered.

The sputtering system studied here is cylindrical and it is best to use cylindrical coordinates to describe neutral transport through the main chamber. The gas-phase transport in the main chamber, in the presence of gas-phase collisions, is the main topic of this paper. The trench transport, on the other hand, is treated here as being collisionless (although this is certainly not necessary with the present method) and if the trench is linear is best described using Cartesian coordinates. The setting up of the transition matrix in each case and the interface between the two regions is described next. Then in Sec. III we describe results and compare them to other numerical schemes [1] and experiments.

II. CALCULATION OF DEPOSITION RATES

The rate of scattering (number per second) of the sputtered particles is calculated, in steady state, by means of the transition matrix T. The matrix describes collisions which occur in the gas phase or when particles hit the walls. We begin with a description of the gas-phase process model.

A. Gas-phase transport

The volume of the chamber is divided into "cells," usually of constant width in each direction. In the cylindrical chamber the coordinates used are (ρ, z) with the azimuthal angle ϕ assumed to be ignorable. The cells are centered on points (ρ_i, z_j), where $\rho_i = (i - 1/2)\Delta\rho$ and $z_j = (j - 1/2)\Delta z$, where $(\Delta\rho, \Delta z)$ are the cell widths in ρ and z, respectively, and i and j are integers labeling the cell.

The transition matrix element $T^{i,j}_{i',j'}$ contains the probability that a particle which had a scatter in the cell (i', j') will have its next scatter in the cell (i, j). If the steady-state scattering rate in each cell is $R(i, j)$, then scattering at the rate $R(i', j')$ in cell (i', j') will contribute scattering at a rate

$$T^{i,j}_{i',j'} R(i',j') \tag{1}$$

in the cell (i,j). The total rate of scattering in (i,j) is obtained by summing over all "initial" cells (i',j') and adding any production or injection of particles in (i',j') with rate $S(i',j')$. Then

$$R(i,j) = \sum_{i',j'} T^{i,j}_{i',j'} (R(i',j') + S(i',j')). \tag{2}$$

Equation (2) is then iterated until the individual $R(i,j)$'s change by less than a user specified amount, typically 10^{-6}.

Collisions with the surface can be included similarly. More details of the method can be found in Ref. [9] and in the Appendix. The model of gas-phase transport is valid, if necessary with minor modifications to include a more detailed description of the collisions, for all long mean free path cases.

The angular distribution of particles can also be found by summing over all initial cells. In this work, we are interested in the angular distribution of particles striking the substrate surface. The procedure to find the distribution is given next.

B. Angular distribution striking the substrate

In the present work, the distribution of scattered particles in the main volume is found first. This region is described in cylindrical coordinates. This allows us to find the angular distribution of particles striking a "point" on the substrate; see Fig. 1. The trench is so small compared to the dimensions of the chamber that it is effectively at a point, from the perspective of the calculation in the main chamber.

Once the main chamber calculation is converged, the angular distribution of particles striking the substrate can be calculated. We consider a point at some radial distance a. We define a set of angles θ and ϕ so that θ is the angle from the z axis and ϕ is the angle from the radial vector $\hat{\rho}$; see Fig. 1. We take a discrete set of values of θ (ranging from 0 to $\pi/2$) and ϕ (ranging from 0 to π), labeled by θ_k and ϕ_l, respectively. For each pair of θ_k and ϕ_l, the distance L in that direction from the point on the substrate to a chamber wall is found. This ray is then divided up into small segments of length Δr. At some distance r along the ray, we identify a volume in the range Δr at r, $\Delta\theta$ at θ, and $\Delta\phi$ at ϕ. The rate of scattering per unit area at the substrate due to this small volume is given approximately by

$$\frac{R(i',j')}{V(i',j')} [r^2 \Delta r \sin(\overline{\theta_k}) \Delta\theta_k \Delta\phi_l] \cos\overline{\theta_k} \frac{\exp(-r/\lambda)}{4\pi r^2}, \tag{3}$$

where $\Delta\theta_k$ and $\Delta\phi_l$ are the widths of the angular bins, $\overline{\theta_k}$ is the average θ in the theta bin, and λ is the mean free path of the particle. The small volume $[r^2 \Delta r \sin(\overline{\theta_k}) \Delta\theta_k \Delta\phi_l]$ is contained in the main chamber cell (i',j'), which has a volume $V(i',j') = \pi\rho_i \Delta\rho \Delta z$. $R(i',j')/V(i',j')$ is the scattering rate per unit volume in (i',j'). For each pair of (θ_k, ϕ_l) the scattering rate is integrated along the ray. The ray will end on the surface

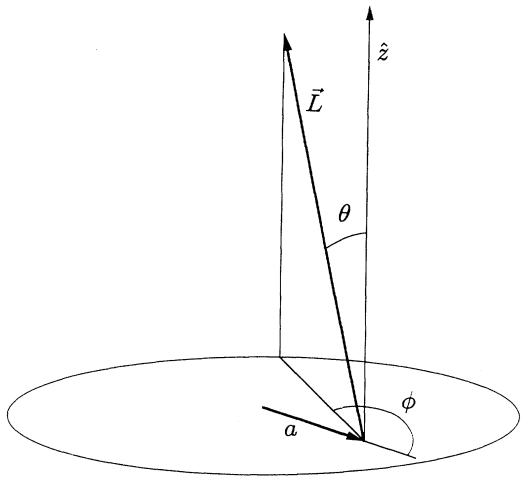

FIG. 1. Calculation of angular distribution of particles striking a surface.

of the chamber wall after the full distance L. Then, the scattering rate per unit area from a chamber wall will contribute

$$\frac{R(i',j')}{S(i',j')} [L^2 \sin(\overline{\theta_k}) \Delta\theta_k \Delta\phi_l] \cos\overline{\theta_k} \frac{\exp(-L/\lambda)}{\pi L^2} \tag{4}$$

at the substrate, where $S(i',j')$ is the area of the chamber wall cell (i',j'). The cosine of the angle made by the ray at the wall enters the angular distribution leaving the cell, but is canceled by the same factor coming from the area of the small wall element in the range $\Delta\theta$ and $\Delta\phi$, expressed in coordinates centered on the substrate at the top of the trench.

C. Transport in the trench

We now turn to the calculation of the transition matrix in the trench T_{trench}. A different approach used previously to calculate the initial deposition rates in the trench in steady-state consists of solving "Clausing-like" integrals [1]. While this approach is similar to the transition matrix (TM) approach described here for the trench, the TM approach is able to connect the trench calculation to the main chamber calculation in a seamless fashion. The former approach assumes an uniform initial flux into the trench, while the TM approach is able to calculate the actual angular distribution of sputtered materials coming into the trench and thereby give more realistic initial deposition rates along the trench walls. There is no assumption about the incoming flux. In fact, this transition from the main chamber calculation to provide the incoming flux to the trench is the main extension needed for calculating the initial deposition profiles in the trench.

The trench is so small compared to the dimensions of the chamber that it is effectively at a point, from the perspective of the calculation in the main chamber. Nevertheless, the length of the trench can be treated as infinite compared to its depth or width.

The sputtered material from the main cylindrical

chamber enters the trench from the top and collides with the walls possibly many times before either exiting or sticking to the trench walls. Neglecting the possibility of reaction in the trench volume or with the trench wall, for the present calculation, we make the following set of assumptions.

(i) The frequency of particle-particle collisions in the trench (not in the main chamber) is negligible relative to particle-wall collisions.

(ii) The open end of the trench has a constant flux of sputtered materials coming from the main chamber, which is found as described above.

(iii) The particles reflect perfectly diffusely from the trench surfaces.

(iv) Surface diffusion inside the trench is negligible. These assumptions are similar to those in Ref. 1.

Due to assumption (i), gas-phase collisions in the trench are negligible (unlike the main chamber calculation where they are essential) and the transition matrix for the trench T_{trench} only involves "transitions" from collisions with one surface of the trench to collisions with other surfaces of the trench. The calculation of T_{trench} can be done analytically and is described in detail next. The angular distribution of the sputtered material entering the trench from the top is found in the main chamber calculation, as shown in Fig. 2. The main chamber part of the calculation treats all boundaries as absorbing some fixed fraction (typically 10% in the cases presented here) of the incoming flux, diffusely reflecting the rest; the source also emits at a fixed rate. The trench is ignored in the main chamber calculation. Once the main chamber calculation is converged, the trench transport is modeled next with the angular distribution entering the trench being the same all across the top. Once particles are in the trench the top "absorbs" all particles that return to it, whereas the walls capture a fraction γ of particles hitting them. A more sophisticated treatment of deposition could be used however; we use a simple phenomenological sticking coefficient to illustrate the trench transport.

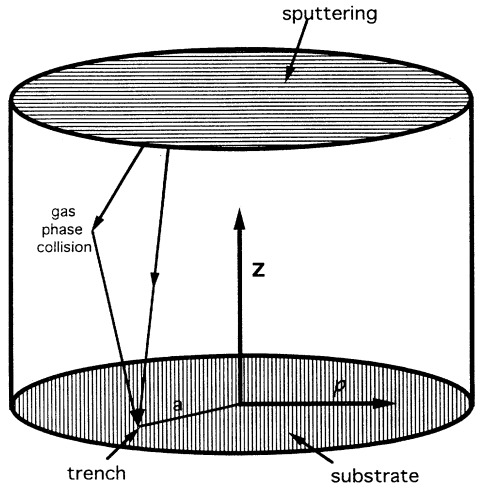

FIG. 2. Chamber geometry.

This implicitly assumes first-order kinetics (i.e., γ is independent of the flux of sputtered particles).

The calculation of T_{trench} uses the geometry shown in Fig. 3. The trench is approximated as being infinite in length and rectangular in cross section. Gas-phase scattering in the trench is ignored, so T_{trench} is the probability of scattering off an element of the wall having previously scattered off another element of the wall. The walls of the trench are divided into infinitely long strips of width Δ. The calculation of T_{trench} can be divided into three

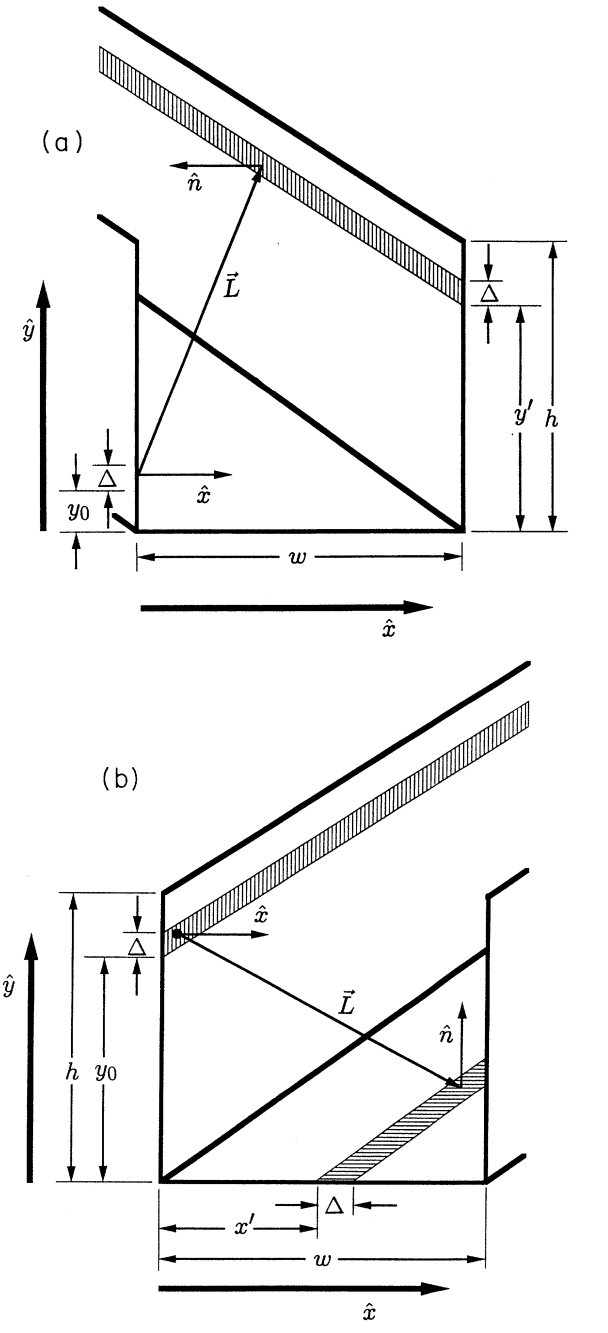

FIG. 3. Trench geometry: (a) particles hitting the parallel wall and (b) particles hitting the perpendicular wall.

parts. First, we find the probability of a particle leaving a trench wall and hitting a parallel wall. Second, we find the probability of a particle leaving a trench wall and hitting a perpendicular wall. Finally, given an angular distribution of particles coming through the top of the trench, we find the probability of striking the trench walls. We consider these cases next.

We start by considering particles starting at a point y_0 on the left trench wall (see Fig. 3). We assume that the angular distribution of the particles leaving the wall is isotropic [assumption (iii)]. Then the probability of the particle hitting an infinitesimal final surface element dS is given by

$$\frac{1}{\pi}\int \frac{\cos(\theta_n)\,\hat{\mathbf{L}}\cdot\hat{\mathbf{n}}}{L^2}\,dS, \tag{5}$$

where θ_n is the angle between $\hat{\mathbf{x}}$, the normal to the initial surface, and the trajectory of the particle. The trajectory is along the unit vector $\hat{\mathbf{L}}$, where $\mathbf{L}$ is the vector from initial point on the surface to the final surface element dS, and $\hat{\mathbf{n}}$ is the vector normal to the final surface element dS. The factor $\cos\theta_n$ ensures an isotropic distribution of the particles leaving the initial surface, while the factor $1/\pi$ is the normalization.

If we first consider the particle hitting the parallel wall, then we have $dS = dy\,dz$, $\hat{\mathbf{n}} = -\hat{\mathbf{x}}$, $L^2 = w^2 + (y-y_0)^2 + z^2$, and $\cos\theta_n = \hat{\mathbf{L}}\cdot\hat{\mathbf{n}} = w/L$. w is the trench width. We then find

$$\frac{w^2}{\pi}\int_{y'}^{y'+\Delta} dy \int_{-\infty}^{\infty} \frac{dz}{[w^2+(y-y_0)^2+z^2]^2}, \tag{6}$$

where y' and $y'+\Delta$ are the lower and upper coordinates of the final cell. Integrating over z and then y we find

$$\frac{1}{2}\left[\frac{y'+\Delta-y_0}{\sqrt{(y'+\Delta-y_0)^2+w^2}} - \frac{y'-y_0}{\sqrt{(y'-y_0)^2+w^2}}\right]. \tag{7}$$

Since the particles do not all start from a point y_0, but uniformly in the initial cell (i.e., between y_0 and $y_0+\Delta$), we average over the initial cell. This gives the final probability as

$$\frac{1}{2\Delta}\left[\sqrt{(y'-y_0-\Delta)^2+w^2} - 2\sqrt{(y'-y_0)^2+w^2} + \sqrt{(y'-y_0+\Delta)^2+w^2}\right]. \tag{8}$$

For particles from the same initial cell which hit the bottom of the trench, the final $dS = dx\,dz$, $\hat{\mathbf{n}} = \hat{\mathbf{y}}$, $L^2 = x^2 + y_0^2 + z^2$, $\cos\theta_n = x/L$, and $\hat{\mathbf{L}}\cdot\hat{\mathbf{n}} = -y_0/L$. First integrating over the final cell (from x' to $x'+\Delta x$) and then over the initial cell, we find the probability

$$\frac{1}{2\Delta}\left[\sqrt{x'^2+(y_0+\Delta)^2} - \sqrt{x'^2+y_0^2} + \sqrt{(x'+\Delta)^2+y_0^2} - \sqrt{(x'+\Delta)^2+(y_0+\Delta)^2}\right]. \tag{9}$$

The probability of going between cells on the bottom and the right wall of the trench can also be found using this expression. The probability of particles going out through the top of the trench can also be found using Eqs. (8) and (9). These expressions, while only valid for a nonevolving trench wall, can be generalized to a wall which evolves in time (see below). Similar integrals have been described in Refs. [1,10,11].

We now turn to finding the probability distribution for particles, coming through the top (from the main chamber) and hitting the trench walls. Since, in general, the angular distribution is not known, analytic expressions cannot be given. However, once an angular distribution is found from the main chamber calculation, it is a straightforward task to find where particles hit the trench walls.

The trajectory of a particle entering the trench makes an angle of θ between the top normal $(-\hat{\mathbf{y}})$ and the trajectory and makes an angle ϕ with the local z axis of the trench. Given the location x where the particle crossed the top of the trench, one can find where the particle will hit a trench wall. For each x value on top of the trench, the fraction of particles striking each cell of the trench walls is computed by integrating over θ and ϕ. After all x values are considered, an average probability is found for particles coming through the top hitting each cell of the trench walls.

III. RESULTS OF SIMULATIONS

In this section we review the results obtained using the transition matrix to describe sputtering, with allowance for transport in the presence of collisions in the main chamber and into the trench. We then compare our results to experiment. However, we first show that the initial deposition rate predicted by our method for an isotropic flux of sputtered material entering the trench is in agreement with the results of Ref. [1].

Figure 4 compares the analytic [1] and transition matrix results for initial deposition rates defined relative to the deposition rate on the exterior of the feature. The aspect ratio of the trench (height to width) is 2 and the sticking coefficient $\gamma = 1.0$. Figure 5 compares the initial deposition rates for the same trench but with various values of γ. The vertical axis in each figure has been normalized to the deposition rate on the exterior of the feature. The horizontal axis is the normalized distance (i.e., x/w or y/h) from the bottom corner of the trench (Fig. 3). All the figures show excellent agreement.

The remaining figures relax the assumption of an isotropic flux of sputtered material entering the trench. Instead, the angular distribution is found from the main chamber calculation. The cathode (Fig. 2) consists of the sputtered material which is titanium. The gas in the main chamber consists primarily of argon. Only titanium sputtered off the cathode is tracked in the main chamber and in the trench. The rate of titanium coming off the cathode is assumed to be uniform in space and constant in time.

First the steady-state scattering rates for the main chamber are found. Any titanium that hits the main chamber's wall is absorbed with a probability of 0.1, the

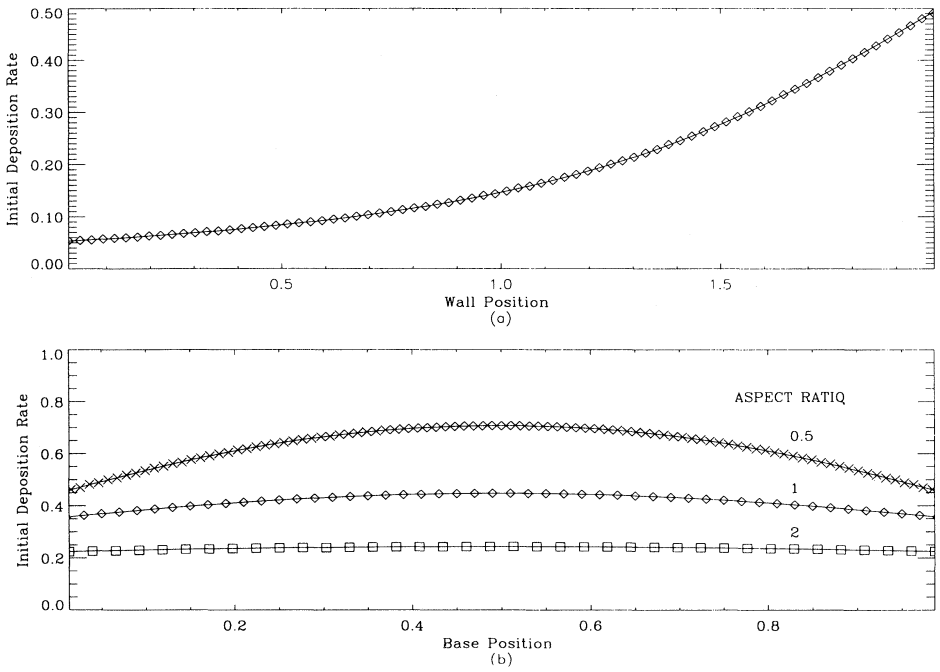

FIG. 4. Initial deposition rate in a trench with $\gamma = 1$: line, Ref. [1]; symbol, transition matrix. (a) Along the trench wall for the aspect ratio h/w of 2; (b) along the trench bottom for various aspect ratios.

rest being reflected diffusely. Once the steady-state distribution is found, the angular distribution at some radius $\rho = a$ on the substrate is found and the propagator that describes how the incoming particle flux is deposited onto the trench walls is computed. Finally, given a value of the sticking coefficient γ, the scattering rates on the walls of the trench are iterated until steady state is achieved.

For the system studied here (Table I), the angular distribution at the substrate at $\rho = 0$ is uniform in ϕ and for small values of θ it is uniform in θ, but there is a sharp decrease in the flux for angles $\theta > \arctan(R/H)$, where R and H are the radius and the height of the main chamber, respectively. This is expected since in this calculation the mean free path of titanium is considerably longer than the main chamber dimension.

For large values of the sticking coefficient $\gamma \simeq 1$, the effect of the anisotropy on the deposition rate is to decrease it near the top of the trench and to increase it on the bottom of the trench compared to the isotropic flux case (Fig. 6). The bottom of the trench receives more material per unit area because the incoming particle flux

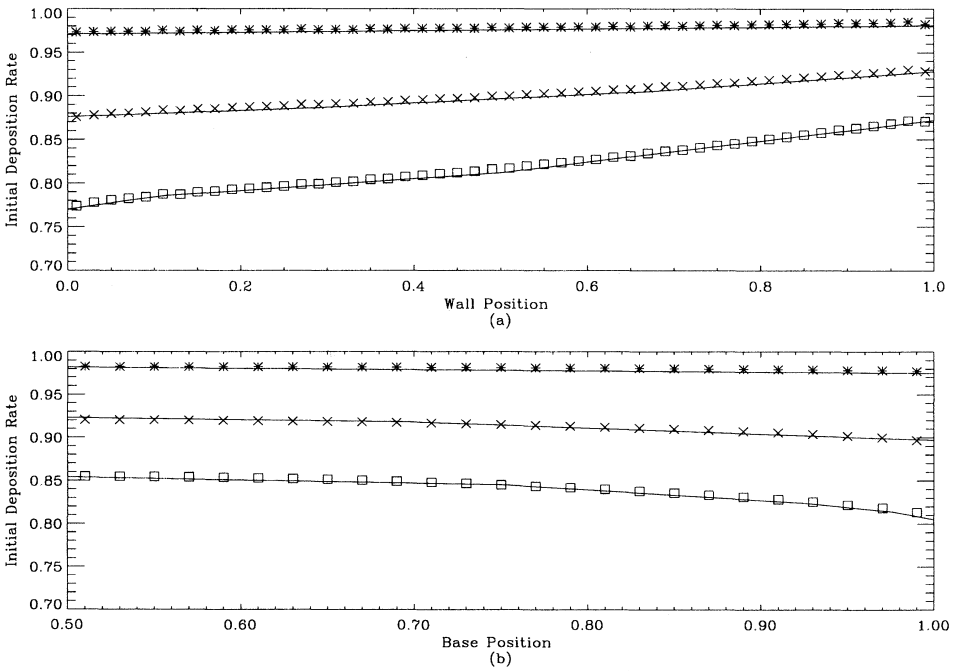

FIG. 5. Initial deposition rate in an $h/w = 1.0$ trench: line, Ref. [1]; symbols, transition matrix. $*$, $\gamma = 0.01$; $\times$, $\gamma = 0.05$; $\square$, $\gamma = 0.1$. (a) Along the trench wall and (b) along the trench bottom.

TABLE I. Parameters used in the simulation.

Quantity	Value	Units
Chamber radius	14.288	cm
Chamber height	5.0	cm
Ti mean free path λ	40.0	cm
Gas temperature	300	K

TABLE II. Comparison of deposition rates.

Aspect ratio h/w	Relative depth of material in experiment	Calculated depth $\gamma = 0.1$	$\gamma = 0.2$	$\gamma = 0.3$
1.25	0.89	0.84	0.72	0.63
1.5	0.66	0.80	0.66	0.57
1.875	0.41	0.74	0.59	0.49

is directed mostly downward into the trench.

For low sticking coefficients $\gamma \simeq 0$, particles achieve a roughly isotropic distribution in the volume near the bottom of the trench and a uniform rate of hitting the walls and bottom (Fig. 7). If the incoming distribution is peaked downwards (into the trench), then for $\gamma \simeq 0$ the deposition rate actually decreases near the top. Since the rate is uniform in the isotropic case, this should be expected. This is because the incoming particles have a "high" probability of going to the bottom of the trench where they are scattered isotropically. When they return to the top the chance of escape increases as they approach the top so the deposition rate drops.

As shown in Table II, the sticking coefficient γ can be estimated by comparing the deposition rate at the center of the bottom of the trench to experiment. Since the evolution of the trench shape is not allowed for, the calculated deposition rate is essentially the initial deposition rate. That is, once titanium is first deposited onto the trench wall, the propagators inside the trench will change. This effect is not included here. While the simulation results have the correct trend in that the deposition rate decreases as the depth increases and also as γ decreases, the numerical results do not show as much variation as the experiments. However, assuming a uniform deposition rate, each wall will "encroach" by equal amounts. Therefore the trench as it evolves effectively becomes narrower faster than it becomes shallower, compounding the low deposition rate on the bottom. This means that the calculated rates are upper limits and so we may deduce that a value of $\gamma \sim 0.1$ or less is reasonable.

Also shown, in Figs. 8 and 9, is the deposition rate at different radii and different orientations, all for $\gamma = 0.1$. Comparing these figures, the deposition rates do not change appreciably with radius until the trench is near the radial outer boundary of the main chamber (Fig. 9). Also, if the trench is rotated so that the trench z axis is not along the main chamber ρ axis, the deposition rates are not strongly effected until, again, the trench is located near the outer radial boundary. Experimentally, little variation with ρ is seen ($< 2\%$) and this may also indirectly point to a low value of γ. The multiple bounces that occur in the trench when γ is low make the flux "forget" its initial angular distribution, which is distorted as ρ increases. As a result, radial effects manifest later for γ near to zero.

While we have only shown results for an infinite rectangular trench, the scheme outlined here can be extended to more complicated geometries. As long as the walls of the trench are parallel, the z integral in Eq. (5) can be done analytically. If one takes the trench as piecewise linear segments, the other integrals can also be calculated either analytically or numerically. Similar approaches

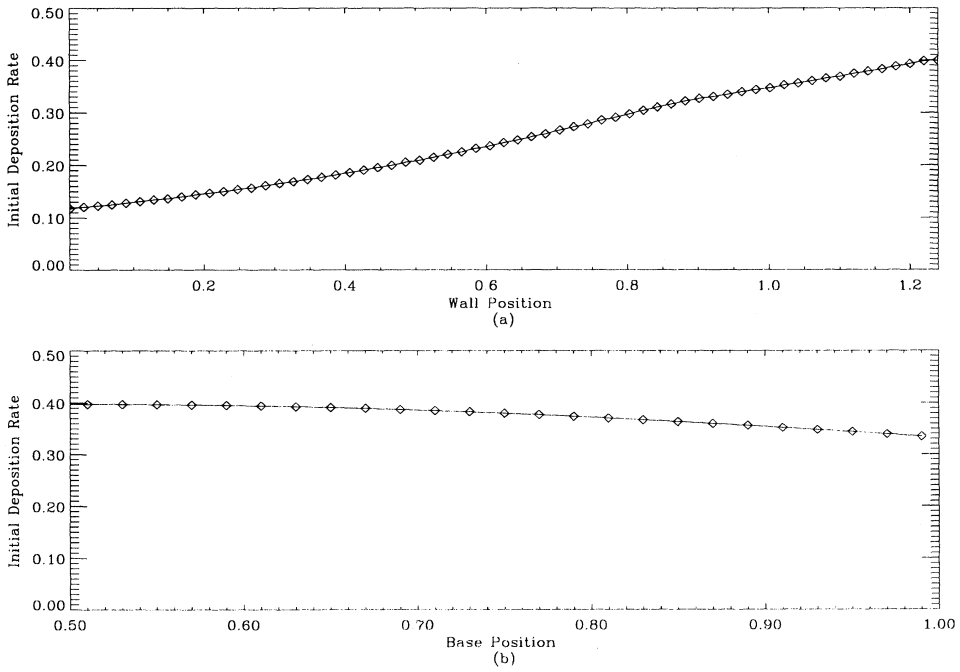

FIG. 6. Initial deposition rate in an $h/w = 1.25$ trench with $\gamma = 1$. (a) Along the trench wall and (b) along the trench bottom.

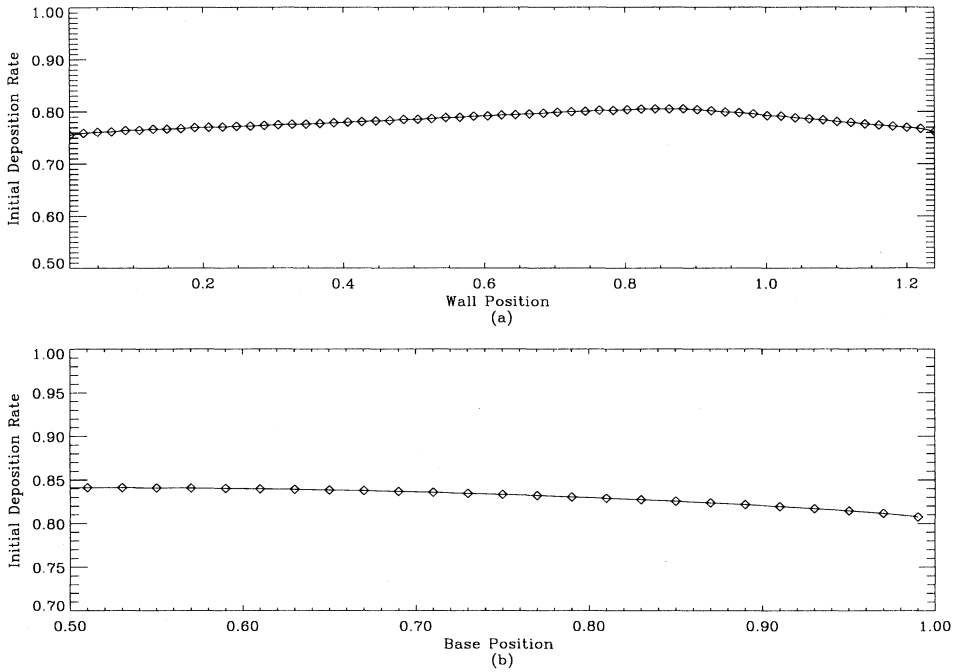

FIG. 7. Initial deposition rate in an $h/w = 1.25$ trench with $\gamma = 0.1$. (a) Along the trench wall and (b) along the trench bottom.

to the calculation inside the trench have been used in Refs. [1,10,11].

In conclusion, we have developed a transition matrix description of gas-phase transport at long mean free path, allowing for gas-phase collisions. Using this method to describe the initial deposition rate of sputtered materials has been shown to be a very efficient means of calculation that is at least as accurate as MC and DSMC methods, since it does not have the statistical errors that the MC method exhibits. The ability to couple the scattering in the main chamber to the angular distribution coming into the trench makes the calculation physically more realistic than previous models of deposition [1]. Because of the simple and efficient algorithm, it can be run as part of a global deposition model. Future work will allow the trench profile to evolve in time.

APPENDIX: NUMERICAL PROCEDURE

The numerical scheme used to calculate the steady-state scattering rate distribution in the main chamber is

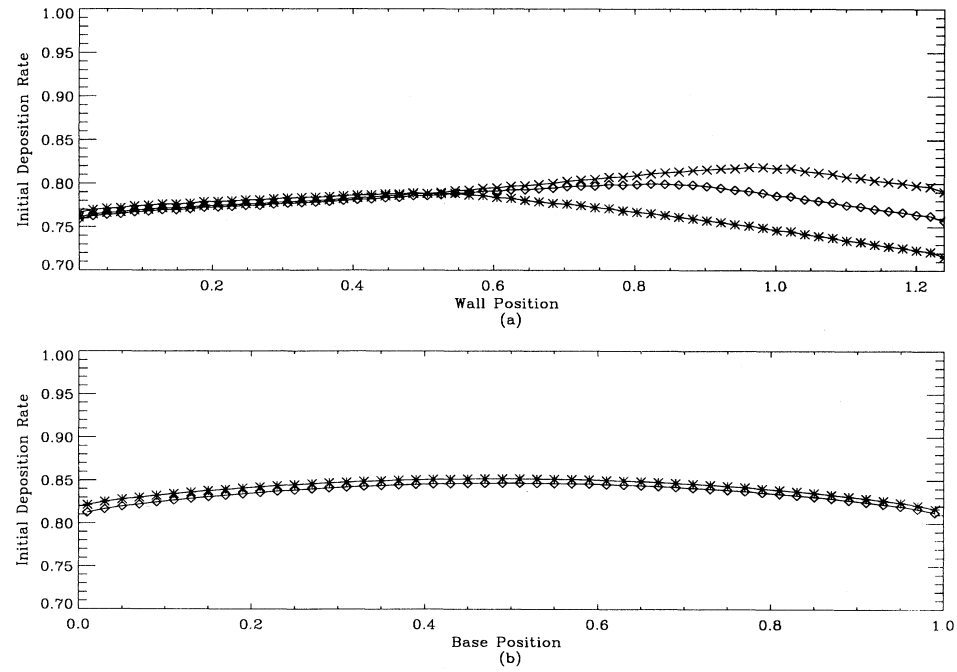

FIG. 8. Initial deposition rate in an $h/w = 1.25$ trench with $\gamma = 0.1$, $\rho = 7.114$ cm, and the angle ϕ' between the trench z axis and the main chamber ρ: $\diamond$, $\phi' = 0$; $\times$, $\phi' = \pi/2$, wall farthest from $\rho = 0$; $*$, $\phi' = \pi/2$, wall nearest to $\rho = 0$. (a) Along the trench wall and (b) along the trench bottom.

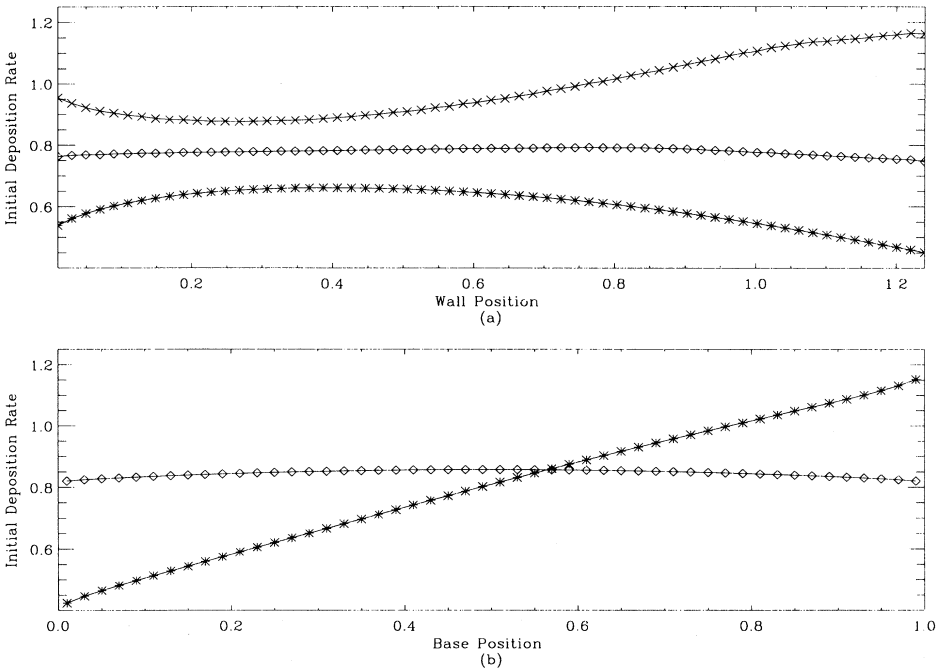

FIG. 9. Initial deposition rate in a $h/w = 1.25$ trench with $\gamma = 0.1$, $\rho = 14.228$ cm, and the angle ϕ' between the trench z axis and the main chamber ρ: $\diamond$, $\phi' = 0$; $\times$, $\phi' = \pi/2$, wall farthest from $\rho = 0$; $*$, $\phi' = \pi/2$, wall nearest to $\rho = 0$. (a) Along the trench wall and (b) along the trench bottom.

described in this appendix. The first step of the calculation is to find the rate R at which particles scatter in each cell of the mesh. Once this is known, it is straightforward to find the distribution function $f(\mathbf{r}, \mathbf{v})$. For this reason, we begin by focusing on the scattering rate. Since R is typically a function of two fewer variables than f, it can be much more effective to do the bulk of the calculations in terms of R. The description of the construction of the distribution function from R is given later in this appendix.

In the present work we use momentum conservation to find a mean z velocity for all particles of a given species that scatter in a particular cell. We assume that the particles of each species are scattered isotropically in the appropriate reference frame moving at the mean z velocity for scattered particles of that species.

The calculation of the scattering rate R will now be described, first assuming that particles scatter off fixed scattering centers and have constant mean free path λ in space and then assuming momentum conservation and a spatially variable λ. The wall scattering is handled in a similar fashion to volume scattering, so we begin with volume scattering and then indicate the differences that occur when the scattering is off the wall.

1. The idealized case

The geometry used here is cylindrical, with symmetry in the azimuthal angle assumed. Other geometries can be handled similarly. We first set up a table of probabilities $T^{i,j}_{i',j'}$. This represents the probability that a particle that scatters in the initial cell (i', j') will have its next scatter in the final cell (i, j). In this section our focus is not on finding T, but how it can be used to describe the neutral species, so we take λ to be constant in what follows next.

The index i refers to the radius $\rho = (i - 1/2)\Delta\rho$, while $z = (j - 1/2)\Delta z$, with $\Delta\rho$ and Δz being the mesh spacings in r and z. If one particle per second scatters in (i', j'), this contributes a scattering rate $T^{i,j}_{i',j'}$ in the cell (i, j). Similarly the scattering rate $R(i', j')$ in the cell (i, j) contributes a scattering rate $T^{i,j}_{i',j'}R(i', j')$ in cell (i, j).

If particles are "created" in cell (i', j'), either by chemical reactions or by injection from outside, with rate $S(i', j')$, then the net flux leaving (i', j') is increased by the amount $S(i', j')$. If a fraction $1 - \alpha_{i',j'}$ of the particles scattering in (i', j') are converted to another species, then instead of the total outward flux of particles of this species scattered in (i', j') being simply $R(i', j')$, we instead have $\alpha_{i',j'}R(i', j')$. The outward flux is thus

$$F(i', j') = \alpha_{i',j'}R(i', j') + S(i', j'). \tag{A1}$$

Summing over all initial cells (i', j'), the total scattering rate in cell (i, j) is then

$$R(i, j) = \sum_{i',j'} T^{i,j}_{i',j'}(\alpha_{i',j'}R(i', j') + S(i', j')). \tag{A2}$$

This equation can be iterated to find $R(i, j)$ in each cell of the mesh.

The idealized table of probabilities can be found analytically. As stated above, for simplicity we begin by assuming isotropic scattering and a constant mean free path. These assumptions can easily be removed, and this will be done below. If the initial cell has volume $\Delta V'$ and the final cell has volume ΔV, if a vector pointing from the origin to a point in $\Delta V'$ is denoted $\mathbf{X}'$ and the vector pointing to a point in ΔV is denoted $\mathbf{X}$, and $\mathbf{R} = \mathbf{X}' - \mathbf{X}$, then

$$T^{i,j}_{i',j'} = \frac{k}{\Delta V'} \int_{\Delta V'} \int_{\Delta V} d^3X' d^3X \frac{\exp(-kR)}{4\pi R}, \tag{A3}$$

where $\lambda = 1/k$ is the mean free path. Alternatively, T can in general be found by a MC calculation. Particles are launched with a uniform distribution throughout $\Delta V'$. Assuming isotropic scattering, $\cos\theta = 1 - 2\eta_1$, $\phi = 2\pi\eta_2$, and the distance traveled before scattering is $R = -\lambda \ln \eta_3$, where the η's are uniformly distributed numbers between 0 and 1. The fraction of the particles that subsequently scatter in cell (i, j) is $T^{i,j}_{i',j'}$.

The walls are also divided into cells. The fraction of the particles from any volume cell (i', j') striking each cell of the wall, either at the ends in z or at the outer radius, is recorded. Similarly, the fraction of particles scattering in any wall cell that go to any other wall cell or to any volume cell is found. Particles leaving cells are (for now) assumed to be distributed isotropically, which means that for volume cells their number leaving in a given range of θ and ϕ is proportional to the area dS on the surface of a sphere in that range of the angles. For surface cells, the distribution is weighted with an extra factor of $\cos\theta_n$, where θ_n is the angle of the trajectory from the normal vector to the surface. In addition, it also weighted with the $\sin\theta$ from dS, making $\sin\theta\cos\theta_n$. In setting up the table T using the MC, we simply need to know the angular distribution, either $P(\theta) = \sin\theta$ or $P(\theta, \theta_n) = \sin\theta\cos\theta_n$, respectively, and normalize this suitably so each particle has unit probability of going to some θ, ϕ. When normalized to a total rate of one particle per second, the number leaving a point in the volume per second in $d\theta$ at θ and $d\phi$ at ϕ is $\sin\theta d\theta d\phi/4\pi$. For a point on the surface, the equivalent number leaving the point is $\sin\theta\cos\theta_n d\theta d\phi/\pi$.

In our cylindrical case the z symmetry of the table is broken only at the end walls. Therefore transition probabilities need only be stored in terms of the difference in z between the pairs of cells (in addition to the initial and final radii ρ' and ρ), considerably reducing the time to set up the table T and its size.

2. The general transition matrix

The table T as described so far is for λ = const. In the reactor, λ is roughly constant but not exactly so. We now discuss ways to allow for variable λ with a "null-collision" method, which is used in the present work. Finally, we sketch a very precise treatment of angular scattering, which will be described fully in future work.

The MC method could be used to generate T for an arbitrary profile of λ, but then the symmetry in z would be lost, so T would be a very large matrix, and T would need to be updated during the calculation of R whenever λ changed. In the null-collision method we find the T matrix corresponding to $\lambda_{\min}$, where $\lambda_{\min}$ is the smallest λ value occurring in the region modeled. In practice we find T for several discrete values of $\lambda_{\min}$, for use in different parts of the discharge. Then in each cell the calculated scattering rate is overestimated by $T(\lambda_{\min})$. This can be corrected using a more accurate value of λ to find how many of the collisions in each final cell were unphysical or null collisions. The particles that had null collisions are considered to have collided with their own species in the momentum-conserving version of the procedure described below. Thus the net velocity of that species is found correctly with some small error in the angular distribution.

If a precise description of scattering for arbitrary λ and arbitrary angular distribution is needed, the transition matrix can be set up more exactly. For a given angular distribution of scattered particles we allow the appropriate fractions of the scattered particles to move along "rays" originating from the cell where scattering occurs. Each ray is described in spherical coordinates as being in the range θ to $\theta + d\theta$ and ϕ to $\phi + d\phi$. As particles move down the ray, they are allowed to scatter at a rate determined by the local mean free path λ. If the calculation is overall being done in Cartesian coordinates, for example, each ray overlaps a series of rectangular cells. The fraction of the beam that has not yet scattered but which scatters in a given Cartesian cell c that overlaps beam b can be written

$$\{\exp(-r/\lambda) - \exp[-(r + \Delta r)/\lambda]\}\, a_{b,c} \sin\theta d\theta d\phi, \qquad \text{(A4)}$$

where λ is the local mean free path which is allowed to vary arbitrarily and the factors $a_{b,c}$ are purely geometrical reflecting the overlap of each beam b with each cell c. They can be stored for use in calculating the transition matrix T, since the elements of T can be found directly from the $a_{b,c}$'s. The $a_{b,c}$'s are independent of the initial cell, in Cartesian coordinates, in which case $a_{b,c}$ is a three-dimensional quantity. In this case normalization is achieved by subtracting the fraction of the remaining particles as each cell is crossed and allowing the rest of the particles to pass through, some ultimately reaching the boundary of the simulation region.

For two dimensions, the propagator would in general be four dimensional, making calculations prohibitively slow, even for a very simple model of the transport process with a well-known propagator. The propagators used here are all compact in that they can all be found efficiently with information stored in three-dimensional form.

3. Momentum conservation

The effect of momentum conservation on the scattered distribution is included next by allowing the scattered particles of each species in each cell to have a different drift velocity $\mathbf{V}_{\rm dr}$, superimposed on their random velocity. In the frame moving with $\mathbf{V}_{\rm dr}$ the scattering is treated as isotropic. $\mathbf{V}_{\rm dr}$ is different for each species, in each cell of the mesh.

There are two aspects to including momentum conservation: the first involves calculating $\mathbf{V}_{\rm dr}$ and the second consists of allowing for $\mathbf{V}_{\rm dr}$ in the transition probabilities used to update R. We begin by discussing how we find $\mathbf{V}_{\rm dr}$, and then turn to the use of $\mathbf{V}_{\rm dr}$ in the calculation of R.

Particles traveling from cell (i', j') to cell (i, j) are assumed to have the thermal speed $V_{\rm th}$ (the particles are monoenergetic in the example given here). Inclusion of an extra energy variable is straightforward. (Since T is known for a range of $\lambda_{\min}$ in any case, the T matrix is not increased in size by including the energy.) The av-

erage z component of velocity of particles scattering in (i,j) is found by averaging over the particles leaving all (i',j') and colliding next in (i,j). This involves the same integration as in Eq. (A3), but with an additional factor of $\cos\theta$ in the integrand, where θ is the angle between the actual velocity and the z axis. This is then multiplied by $mV_{\rm th}$, where m is the particle mass, to find the z momentum brought into (i,j) by particles from (i',j') which scatter in (i,j).

For a single species scattering off itself, the net z momentum of particles scattered in (i,j) is simply obtained by summing this over all (i',j'). For multiple species we consider what fraction of the collisions of species a are with species b to determine the force they exert on each other. In either case, $\mathbf{V}_{\rm dr}(i,j)$ for particles of each species, scattered in (i,j), is chosen to conserve z momentum.

We now turn to the modification of the transition probabilities due to $\mathbf{V}_{\rm dr}$. The calculation done here is for steady state and the time of flight from (i',j') depends on their separation. Further, different parts of the two cells are at different distances. We find the average distance $\overline{R}$ by again using an integral such as Eq. (A3), but with an extra R in the integrand and normalized by dividing by $T^{i,j}_{i',j'}$. The average time of flight is then $t_{\rm fl} = \overline{R}/V_{\rm th}$ and the average additional displacement in z is

$$\delta z = \mathbf{V}_{\rm dr}\overline{R}/V_{\rm th}, \tag{A5}$$

where $\mathbf{V}_{\rm dr}$ is the drift velocity of scattered particles at the initial cell (i',j').

A better approximation would be to find a range of δz values along with a weighting factor associated with each δz. This did not seem warranted at present, but can readily be included if appropriate.

We have now established how we find δz for particles traveling between a certain pair of cells. This is the change in the z position due to the flow velocity $\mathbf{V}_{\rm dr}$. This is in addition to the z motion of isotropically distributed particles in the laboratory frame of reference. As stated above, we assume δz is small. To find δz in this way, we need to know the final cell. We move particle fluxes from the initial cell to the cells which would be the final cells if $\mathbf{V}_{\rm dr}$ were zero. These cells will be "intermediate" cells. We use the same probabilities for going to these intermediate cells as if $\mathbf{V}_{\rm dr}$ were zero.

Having replaced the particle fluxes on the mesh, using the matrix T to find the probabilities and thus ensuring exact normalization, we can shift these intermediate cells by δz. δz is different for each intermediate cell. If for a particular pair of initial and intermediate cells δz carries the intermediate cell 30% of the distance into the next cell, then 30% of the collisions of particles from the initial cell which were indicated for that intermediate cell will take place in the next cell. The remaining 70% take place in the same cell as the intermediate cell. This second step also guarantees exact conservation of the particle fluxes.

The treatment of the shift δz near the ends of the cylinder requires further consideration. We consider separately the cases where δz is towards the end and where δz is away from it. If δz is towards the end we do the first step as usual, using T to move particle fluxes to intermediate cells. Some of the particles strike the end. We assume those strike at approximately the right radius. Then when δz is allowed for, more particles strike the end at the radius of their intermediate cell. This too is approximately correct.

If δz is away from the end, the first step is done as usual. We also keep track of the scattering rate in an imaginary volume cell behind the end. Then when δz is allowed for, some fraction of the imaginary cell is moved into the solution region. The scattering rate on the surface, at that radius, is decreased by the amount of scattering shifted into the volume next to the surface. The scattering rate added to the volume at each radius cannot exceed that which was on the surface. This procedure is essentially the converse of what is done for the opposite sign of δz. Since δz is expected to be especially small near the ends, in most cases, these approximations should be valid.

For the purpose of finding the $\mathbf{V}_{\rm dr}$ carried from the initial cell (i',j') to the final cell (i,j), the particles are all treated as originating in (i',j'). The actual number going to (i,j) from (i',j') is changed by having a nonzero $\mathbf{V}_{\rm dr}$, but the angle is not changed.

[1] T. S. Cale, G. B. Raupp, and T. H. Gandy, J. Appl. Phys. **68**, 3645 (1990); T. S. Cale and G. B. Raupp, J. Vac. Sci. Technol. B **8**, 649 (1990); T. S. Cale, T. H. Gandy, and G. B. Raupp, J. Vac. Sci. Technol. A **9**, 524 (1991).

[2] C. E. Wickershan, J. Vac. Sci. Technol. A **5**, 1755 (1987).

[3] M. J. Cooke and G. Harris, J. Vac. Sci. Technol. A **7**, 3217 (1989).

[4] A. Yuuki, Y. Matsui, and K. Tachibana, Jpn. J. Appl. Phys. **28**, 212 (1989).

[5] R. N. Tait, S. K. Dew, T. Smy, and M. J. Brett, J. Vac. Sci. Technol. A **10**, 912 (1992).

[6] S. Igarashi, K. Nanbu, S. Mitamura, and T. Sugawara (unpublished).

[7] D. Coronell and K. Jensen, J. Electrochem. Soc. **139**, 2264 (1992).

[8] A. Kersch, W. Morokoff, Chr. Werner, D. Restaino, and B. Vollmer, in *International Electron Devices Meeting* (IEEE, New York, 1992), p. 181.

[9] R. E. P. Harvey, W. N. G. Hitchon, and G. J. Parker, J. Appl. Phys. **75**, 1940 (1994).

[10] E. S. G. Shaqfeh and C. W. Jurgensen, J. Appl. Phys., **66**, 4664 (1989).

[11] V. K. Singh, E. S. G. Shaqfeh, and J. P. McVittie, J. Vac. Sci. Technol. B **10**, 1091 (1992).